The Journal of Chemical Physics

The excited states of azulene: A study of the vibrational energy levels for the lower ππ*-valence states by configuration interaction and density functional calculations, and theoretical studies of the Rydberg states

Cite as: J. Chem. Phys. **157**, 154307 (2022); https://doi.org/10.1063/5.0106697
Submitted: 29 June 2022 • Accepted: 20 September 2022 • Accepted Manuscript Online: 20 September 2022 • Published Online: 20 October 2022

Michael H. Palmer, Nykola C. Jones, Søren Vrønning Hoffmann, et al.

The Journal of Chemical Physics ARTICLE scitation.org/journal/jcp

The excited states of azulene: A study of the vibrational energy levels for the lower ππ*-valence states by configuration interaction and density functional calculations, and theoretical studies of the Rydberg states

Cite as: J. Chem. Phys. 157, 154307 (2022); doi: 10.1063/5.0106697
Submitted: 29 June 2022 • Accepted: 20 September 2022 •
Published Online: 20 October 2022

Michael H. Palmer,[1,a] Nykola C. Jones,[2,b] Søren Vrønning Hoffmann,[2,b] R. Alan Aitken,[3,b] Marcello Coreno,[4,b] Monica de Simone,[5,b] Cesare Grazioli,[5,b] and Iain L. J. Patterson[3,b]

AFFILIATIONS

[1] School of Chemistry, University of Edinburgh, Joseph Black Building, David Brewster Road, Edinburgh EH9 3FJ, Scotland, United Kingdom
[2] ISA, Department of Physics and Astronomy, Aarhus University, Ny Munkegade 120, DK-8000 Aarhus C, Denmark
[3] School of Chemistry, University of St Andrews, North Haugh, St. Andrews, Fife KY16 9ST, Scotland, United Kingdom
[4] ISM-CNR, Instituto di Struttura della Materia, LD2 Unit, 34149 Trieste, Italy
[5] IOM-CNR, Istituto Officina dei Materiali, Basovizza SS-14, Km 163.5, 34149 Trieste, Italy

[a] **Author to whom correspondence should be addressed:** m.h.palmer@ed.ac.uk
[b] **Electronic addresses:** nykj@phys.au.dk; vronning@phys.au.dk; raa@st-andrews.ac.uk; marcello.coreno@elettra.eu; desimone@iom.cnr.it; grazioli@iom.cnr.it; iljp@st-andrews.ac.uk

ABSTRACT

A new vacuum ultraviolet absorption (VUV) spectrum of azulene vapor has been obtained by using a synchrotron radiation source. The onset of the ultraviolet spectrum, previously reported by Sidman *et al.*, has been analyzed in detail by Franck–Condon (FC) and Herzberg–Teller (HT) methods. The photoelectron spectral profile identifies the 3px-Rydberg state 0^0 band to be 131 cm^{-1} from the VUV maximum. Excited state energy levels were calculated by three independent methods: the wide scan VUV spectrum was correlated with symmetry adapted cluster configuration interaction calculations. The low energy portion of the spectrum was studied by both time dependent density functional theoretical methods (TDDFT) and multi-reference multi-root CI (MRD-CI). Equilibrium structures were determined for valence states at the TDDFT level. Rydberg states were determined by both TDDFT and MRD-CI. The FC + HT analyses were performed on the TDDFT wavefunctions. The HT intensity profiles are generally low in intensity, relative to the FC ones; however, HT is dominant in the second singlet state (S_2, 1^1A_1). As a result, numerous non-symmetric modes, their overtones, and combination bands show considerable intensity in that band. Energies obtained from use of extremely diffuse s-, p-, d-, or f-character functions enabled realistic extrapolation to the IE_1 for many Rydberg states (RS). The lowest RS ($3b_13s$) based on IE_2 lies at 4.804 eV with a quantum defect of 0.714. Differentiation between valence and RS is readily made using the second moments of the charge distribution.

I. INTRODUCTION

Recently, we reported synchrotron based, vacuum ultraviolet (VUV) absorption and high-resolution photoelectron spectra (PES) spectra for some multiply conjugated molecules, including cyclooctatetraene (COT),[1,2] cycloheptatriene (CHT),[3,4] and norbornadiene (NBD).[5,6] A major difference from preceding work for these high profile molecules is that we have offered interpretations of

the vibrational structure observed in their spectra. We now report a related UV and VUV study of azulene (**1**), another fully conjugated molecule, shown in Fig. 1; recently, we analyzed the vibrational aspects of its PES spectrum.[7] Azulene is isomeric with naphthalene; these two substances played an important part, both in the development and the acceptance of, molecular orbital (MO) theory in the 1940s onwards, and have been the topic of many historical studies.[8–13]

The five visible and ultraviolet band systems found in azulene correspond, with respect to vibrational structure, intensity, and sequence, to the five found in naphthalene, except that the former are shifted to lower frequencies by ~9000 cm^{-1}. The lowest band is shifted even more, ~17 000 cm^{-1}, and its absorption gives azulene its blue color (hence the name). Early molecular orbital calculations for the excited $\pi\pi^*$-states of azulene were based on the Hückel molecular orbital procedure (HMO) that included all singles configuration interaction (CI), a considerable advance to the theoretical procedures available at that time.[14] We now consider the valence and Rydberg states of azulene separately.

A. Valence states

Microwave spectral (MW) studies of the ground X^1A_1 state of azulene show a planar structure with C_{2V} symmetry.[15,16] For the purposes of the present paper, the molecule is oriented with the long, transverse and out-of-plane axes as z, y, and x, respectively; several early papers transposed y and x;[14] we have relabeled their B_1 states as B_2 in the present paper. The spectroscopy of azulene (up to February 1985) was critically reviewed by Robin.[17,18] Five main bands present in the absorption spectrum have onsets at 1.770 ($^1B_2$, S_1), 3.565 ($^1A_1$, S_2), 4.229 ($^1B_2$, S_3), 4.392 ($^1A_1$, S_4), 5.166 eV ($^1B_2$, S_5),[19–21] all attributed to $\pi\pi^*$-valence states; minor variations on these values are reported by other authors.[17,18] The relative oscillator strengths for these lowest bands are 0.01, 0.06, 0.4, 1.0, and ~0.0, respectively. Both $^1A_1$ and $^1B_2$ transitions are optically allowed with electric dipole transition moments along the z- and y-axes.

The HMO calculations above[14] gave a reasonable interpretation of the $\pi\pi^*$-states, both for energy and intensity. The lowest energy one (S_1), responsible for the blue-violet color (λ_{max}700 nm)[14] continues to 450 nm (2.755 eV). The absorption and emission spectra of azulene studied as a solid solution in naphthalene at 20 K show very high resolution.[22,23] The spectra are both polarized and sharp, with 0–0 bands for the two lowest excited states at 1.817 and 3.478 eV (14 652 and 28 050 cm^{-1}). Absorption spectra of jet-cooled azulene for the range up to 2.1 eV provides the highest resolution of the onset ($S_0 \rightarrow S_1$).[24,25] Fluorinated hydrocarbon solutions of azulene enable differentiation of Rydberg from valence states.[26–28] Azulene exhibits fluorescence,[29–33] but contrary to most examples, where emission proceeds to the ground state from the lowest singlet or triplet state (Kasha's Rule), there is practically no S_1 fluorescence, while strong emission occurs from S_2.[34] This significant deviation from the rule was first attributed to the large gap between S_1 and S_2, which allows more internal conversion and vibrational relaxation. A CASSCF study of the S_0 and S_1 surfaces of azulene, by Bearpark *et al.*,[35] showed an S_1/S_0 conical intersection. This crossing established how relaxation, observed by ultrafast S_1 femtosecond decay using laser and spectroscopic linewidth measurements, occurred. The $S_0 \rightarrow S_1 \rightarrow S_2$ excitation pathway has recently been studied by two-dimensional electronic spectroscopy.[36] Fluorescence excitation and dispersed spectra from the S_2, S_3, and S_4 states, when jet-cooled, only show extensive vibrational structure for the S_2 state.[34]

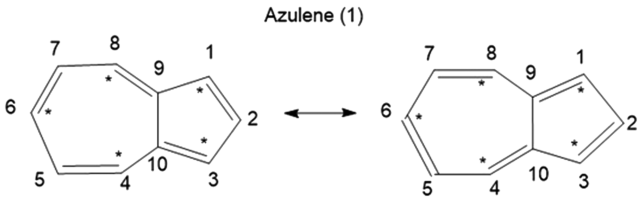

FIG. 1. Azulene (1), as the name implies, is bright blue, an unusual hydrocarbon property. The non-alternant hydrocarbon skeleton is shown by the starred atoms; two adjacent starred or un-starred atoms must arise from the 5 + 7 membered ring atoms. In this study, the axis through C_2C_6 and parallel to C_9C_{10} are z- and y-axes, respectively; the x-axis (π) lies perpendicular to both.

B. Rydberg states

The presence of Rydberg series (RS) in the VUV spectrum of azulene has been widely observed.[37–40] The lowest ionized state of azulene (X^2A_2), energy 7.431(6) eV;[7] was first evaluated by energy extrapolation from these RS[38] as discussed below; direct measurement using He(I) irradiation (584 Å) gave 7.42(5) eV.[41] Two series of VUV RS, also with a limit at 7.431 eV (59 940 cm^{-1}),[38] lead to principal quantum numbers (PQN, n) 4–10 and 4–7, with apparent quantum defects (δ) 0.91 and 1.01. The same peaks[37] have been analyzed in terms of δ = 0.88 and 0.36 for series with n = 4–10 and with 4–5. No peaks were observed in either study for n = 3,[37,38] but these would lie under the strongest band with maximum near 4.773 eV (38 500 cm^{-1}), which contains the S_3 and S_4 $\pi\pi^*$-valence states, as discussed below. Robin[17,18] assigned these two RS as nD, with overall δ = −0.09 and −0.12, respectively; negative δ values were noted as consistent with those for naphthalene. These assignments were attributed to the processes: $2a_2 \rightarrow nd_{XY}$ ($X^1A_1 \rightarrow {}^1A_1$) and $2a_2 \rightarrow nd_{XZ}$ ($X^1A_1 \rightarrow {}^1B_2$).[39,40]

Rydberg states have also been directly obtained by both single and multi-photon excitation (MPI).[42,43] A variation is to use three-photon laser ionization to generate azulene super-excited states; these undergo internal conversion, i.e., relaxation, to generate Rydberg states, which were observed using a further laser.[42] Using these MPI methods various Rydberg states, identified by their quantum defects, were obtained for both azulene and naphthalene with $\boldsymbol{n}$ = 4, 5, and 6.[42,43] These methods do not involve the IE directly so that the Rydberg state energies are relative to the IE, and described as binding energies. Another pump–probe photoionization of azulene showed the ionization process to be more complex but led to six new Rydberg states in the energy range of 4.72–6.33 eV;[44] the δ-values for these new states were assigned to $3p_X$, $3p_Y$, $3d_{XY}$, $3d_{XZ}$, $4p_X$, and $4p_Y$.

Some previous authors[43] had assigned the states with highest δ (e.g., 0.83) as 4s, but given that IE_1 is X^2A_2, that last assignment appears to be incorrect, since these ns-Rydberg states are forbidden. These results suggest a photoionization process that is

driven by an unstable electronic state, possibly a doubly excited state below the ionization potential.[44] The S_2, S_3, and S_4 excited states have very short lifetimes and undergo rapid internal conversion to high vibrationally excited levels of the electronic ground state (S_0*).[45]

The lowest singlet states of azulene (S_n, where n = 1–5) were initially measured directly as $S_0 \rightarrow S_n$ processes by Mann *et al.*[46] Two-photon absorption in the range of 4.067–5.207 eV then led to the consecutive excitation processes $S_0 \rightarrow S_1 \rightarrow S_n$ (n > 1).[47] Synchronous nitrogen and dye laser excitation gave energies from the S_1 to S_3 and S_4.[48] The excitation energies for all of the S_n series (n = 1–5) are comparatively close to the earliest calculations by Pariser.[14]

Ground state vibrational analyses of azulene have been reported using density functional methods (DFT) and basis sets of similar quality to the present study.[49–52] Several analyses of the vibrational structure for excited singlet states of azulene both by fluorescence and absorption have been reported.[23,53,54] Some others include prominent vibrations for the S_2, S_3, and S_4 states of azulene itself, in hydrocarbon solutions at low temperature.[26,27,28]

The main focus of this paper is to offer a detailed analysis of the spectral bands using both Franck–Condon (FC) and Herzberg–Teller (HT) procedures; none have been reported previously for azulene. Our high-level theoretical studies include symmetry adapted cluster (SAC-CI) calculations, time dependent density functional theoretical methods (TDDFT) procedures, and multi-reference multi-root CI (MRD-CI) studies, as described below. We conclude by showing how very diffuse gaussian type orbitals can be used to generate short Rydberg series, which in turn can be extrapolated to generate realistic ionization energies.

II. METHODS

The azulene sample, CAS registry number 275-51-4, was used without further purification; its ^{1}H NMR study showed >99% purity.

A. The UV-visible (UV-vis) and VUV absorption spectrum of azulene

The UV–vis spectral onset was accessed in two ways. Solid azulene, in a 10 cm path-length quartz cell within a Thermo Unicam UV340 instrument, was allowed to equilibrate at room temperature for 48 h before the gas phase measurements commenced. The band-pass and data intervals were 1 and 0.5 nm, respectively, with a scan rate 30 nm/min. Alternatively, we obtained the UV spectrum using a Thermo Evolution 300 spectrometer with a purpose built heated holder, also for a 10 cm quartz cell. The spectrum obtained at 50 °C gave an improved signal to noise ratio over the room temperature data, while still keeping the temperature of the body of the cell low; this avoided azulene condensation on the end windows of the cell. These data were recorded in the spectral range from 800 to 300 nm with a band pass of 0.5 nm intervals at a scan rate of 30 nm/min.v

The spectral range from 340 nm (3.647 eV) to 115 nm (10.781 eV) was collected on the AU-UV beamline of ASTRID2 (Aarhus, Denmark) at 35 °C; at this temperature, the highest sample pressure achievable was 0.02 Torr.[4,6] Data were recorded in steps of 0.05 or 0.1 nm, depending on the level of fine detail in the spectrum. The total energy range was covered by 3131 data points. It is effectively identical to that of Bouler *et al.*[39] over the common energy range of 5.50–7.50 eV, but the much higher cross section has allowed us to expand sections by greater amounts. The combined UV (in blue) + VUV (black) spectra are superimposed on the VUV spectrum and symmetry-adapted cluster configuration interaction (SAC-CI) calculations (Fig. 2).

A more detailed comparison with the jet-cooled two-color multi-photon ionization spectrum (MPI)[24] is shown in the supplementary material (SM), Figure SM1. Many of the principal bands are similar, but our UV340 results are limited to a small number of scans, involving manual collection, and by the very low sample vapor pressure.

B. Theoretical methods

1. General procedures

Several computational chemistry suites were used. Our principal choice was GAUSSIAN-16 (G-16);[56] this contains SAC-CI,[57–61] and the Pisa-group[62–64] software for Franck–Condon (FC) and Herzberg–Teller (HT) vibrational analyses. Input wavefunctions for the FC + HT analyses were obtained by TDDFT methods;[65–67] the Becke three-parameter Lee–Yang–Parr (B3LYP) hybrid functional,[68] including the Coulomb-attenuating method (CAM-B3LYP),[69] was particularly useful. In G-16, adiabatic ionization energies (AIE) are based upon energy differences between ground and excited state *at the excited state equilibrium geometry*; spectroscopic AIE have the difference in energy between

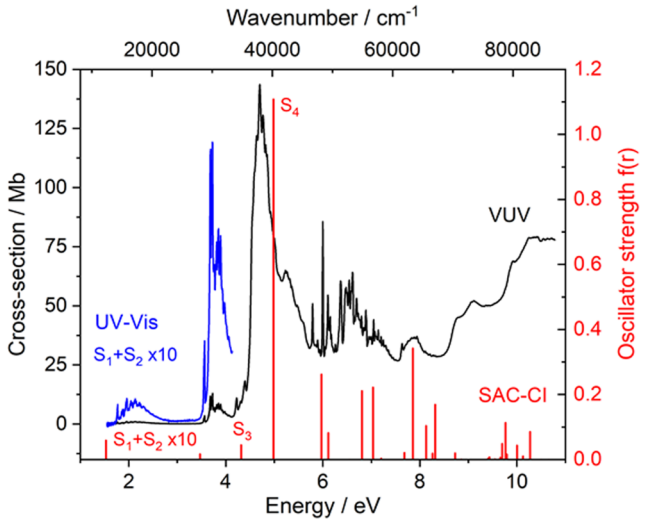

FIG. 2. The wide scan visible + ultraviolet and vacuum ultraviolet spectrum, shown in blue and black, respectively, where the amplitude of the UV–vis cross section has been increased by a factor of 10, to improve its visibility relative to the VUV cross section. The symmetry-adapted cluster calculations (SAC-CI), described in the text, also show a wide range of oscillator strengths, especially near the onset with states S_1 and S_2 and are also amplified by a factor of 10 to improve their visibility.

the excited state and the ground state, *each at their equilibrium structures*.

Azulene is unusual at both the Hartree–Fock and multiconfigurational wave function level[50] in showing a double minimum energy surface; the C_{2V} structure is a maximum and exhibits an imaginary vibration frequency. Density functional methods, originally designed to take into account dynamical correlation, also succeed in these circumstances by generating only positive vibration frequencies.

2. Rydberg states

These were performed by two methods: TDDFT calculations with the CAM-B3LYP method, and the MRD-CI method[70] within GAMESS-UK.[71] The 6-311G(d, p)[72] basis set was augmented by diffuse functions on the azulene a-axis at C_2, thereby maintaining C_{2V} symmetry; this requirement is non-ideal, but G-16 does not allow optimization and frequency determination when functions are on non-atomic centers. The diffuse Gaussian exponents (0.021, 0.008, and 0.002 67), together with s-, p-, d-, and f-spherical harmonics, were as used in our previous Rydberg state determinations. The basis functions were positioned at the center of the C_9C_{10} bond when using GAMESS-UK.[71]

III. RESULTS AND DISCUSSION

General points. Following Pariser,[14] many early papers used the convention that molecules with C_{2V} symmetry lay in the x- and z-plane; this later changed to the y- and z-plane. Here, azulene has out-of-plane π-molecular orbitals (MOs) in the x-axis; similarly, ππ* electronic states, previously of $A_1 + B_1$ symmetry, here are $A_1 + B_2$. Early published assignments have been transposed to the present convention. In summary, the azulene molecule is oriented with rotational constants (A, B, C) in coordinate axes: A(z), B(y), and C(x).

The doubly occupied MOs are σ-MOs: $17a_1 + 12b_2$, and π-MOs: $3b_1 + 2a_2$. The C_{1s} core orbitals, $6a_1 + 4b_2$ although included in all calculations, are ignored in the valence shell labeling system used here, which consists of $11a_1 + 8b_2 + 3b_1 + 2a_2$. Azulene has 48 fundamental vibrations: $17a_1 + 6a_2 + 9b_1 + 16b_2$.

We concentrate on the four-lowest singlet valence states (VS), S_1 to S_4; their polarization gave previous assignments as 1^1B_2, 1^1A_1, 2^1B_2, and 2^1A_1, respectively. We use single excitation configuration interaction (SCI) in TDDFT, with the CAM-B3LYP functional in the FC + HT analyses. These analyses were performed by the Pisa software, as noted in Sec. II B 1.[62–64]

All calculated Rydberg states are preceded in the state singlet manifold by S_1 to S_4; the leading configurations of these are shown in Eq. (1). All of these states are ππ* rather than σσ* excitations and are permutations of the two highest occupied and lowest unoccupied MOs (HOMOs and LUMOs, respectively). Judicious selection of the reference configurations enabled these VS to be de-selected from the CI state expansions using MRD-CI, since these behave as intruder states.

Leading term densities [see Eq. (1)] at the X^1A_1 equilibrium structure, using valence shell numbering and listed by increasing binding energy. These include all the ππ*-states making significant contributions to the cross section of the VUV absorption spectrum; an optically forbidden state in FC terms, 1^1A_2 state is included to demonstrate its relatively low position in the sequence,

$$S_1\,(1^1B_2) : 0.702\,(2a_24b_1^*) + 0.122\,(3b_13a_2^*),$$

$$S_2\,(1^1A_1) : 0.586\,(2a_23a_2*) + 0.394\,(3b_14b_1^*),$$

$$S_3\,(2^1B_2) : 0.651\,(3b_13a_2^*) + 0.243\,(1a_24b_1^*),$$

$$S_4\,(2^1A_1) : 0.584\,(3b_14b_1^*) - 0.396\,(2a_23a_2^*),$$

$$S_5\,(3^1B_2) : 0.649\,(1a_24b_1^*) - 0.204\,(3b_13a_2^*) + 0.139\,(2a_25b_1^*),$$

$$S_6\,(1^1A_2) : 0.646\,(2a_25b_1^*) - 0.193\,(2a_213a_1^*),$$

$$S_9\,(3^1A_1) : 0.600\,(1a_23a_2^*) - 0.311\,(2b_14b_1^*) + 0.120\,(3b_14b_1^*). \quad (1)$$

A. The wide scan VUV spectrum and SAC-CI assignment

We have amplified the spectral cross sections and their calculated oscillator strengths f(r) for the two lowest lying states by a factor of 10; all higher energy calculated results in Fig. 2 have intensities shown in the figure axes. By far the highest cross section is S_4; some of its vibrational structure is associated with the very weak S_3 band, close to 4.3 eV. The relatively sharp set of bands between 5.8 and 7.8 eV are all Rydberg state structure and are discussed separately below.

The lowest SAC-CI singlet (vertical excitation) states, shown in Table I, are determined at the equilibrium geometry of the X^1A_1 ground state. The full set of calculated singlet state energy levels, as depicted in Fig. 2, are shown in the supplementary material (Table SM2). The changes in signs of the transition dipole direction are apparent in Table I. The $^1B_1$ states have non-zero f(r), but most are very small; $^1A_2$ states have f(r) = 0; the πσ*, σπ* states have little influence. This leads to the VUV absorption spectrum being largely dominated by the $^1A_1$ and $^1B_2$ states.

B. The wide scan experimental UV + VUV spectrum

The black curve in Fig. 2 presents the full photoabsorption spectrum of azulene in the range of 1.55–10.78 eV; the UV onset region (in blue) intensity was scaled, as above. The absorbance data measured using the benchtop UV spectrometer have been scaled to the AU-UV beamline intensities in the 3.65–4.13 eV overlap region, in order to present their cross sections in Mb. This spectrum covers the largest energy range with associated absolute cross sections for azulene. Robin[17,18] reviewed many azulene Rydberg states (RS), as stated above. The lowest observed RS, term value 1.549 eV and f(r) 0.024, was assigned to an unspecified $2a_23d$ state, since the 3s states are forbidden. 3p-RS are ~4.339 eV,[39,40] close to the intense ππ*-valence state at 4.711 eV. Two further RS[37,38] also converge on the

TABLE I. The lowest group of SAC-CI singlet state energy levels, as depicted in Fig. 2, together with the state properties such as transition dipole moment and direction, and oscillator strength. The X^1A_1 ground state has calculated dipole moment (+)0.4893 (z) a.u. (1.2444 D).

Energy (eV)	Transition dipole (a.u.)	Oscillator strength	Symmetry	Energy (eV)	Transition dipole (a.u.)	Oscillator strength	Symmetry
1.532	0.3979(*y*)	0.0059	$^1B_2$	6.566	0.0089(*x*)	0.0	$^1B_1$
3.469	0.1434(*z*)	0.0017	$^1A_1$	6.804	1.1246(*y*)	0.2108	$^1B_2$
4.314	−0.6483(*y*)	0.0444	$^1B_2$	7.035	1.1340(*z*)	0.2216	$^1A_1$
4.980	3.0138(*z*)	1.1081	$^1A_1$	7.203	0.1271(*x*)	0.0029	$^1B_1$
5.969	−1.3387(*y*)	0.2621	$^1B_2$	7.681	0.3344(*x*)	0.0210	$^1B_1$
6.115	0.7383(*z*)	0.0817	$^1A_1$	7.857	−1.3333(*y*)	0.3422	$^1B_2$
6.548	−0.0187(*x*)	0.0001	$^1B_1$	8.131	−0.7204(*z*)	0.1034	$^1A_1$

lowest IE at 7.420 eV, but with δ = 0.36 and 0.88; the latter, too high to be an np-Rydberg state, was attributed to a d-series, with higher PQN.[17,18] Higher valence states underlying these Rydberg states are exposed by hydrocarbon solutions, and have broad maxima close to 5.976, 6.509, and 6.980 eV, respectively;[17,18] these energies are very close to those for valence states determined by the SAC-CI method shown in Fig. 2; they correspond to 3^1B_2, 4^1B_2, and 4^1A_1 with energies 5.943, 6.670, and 7.010 eV, respectively. The peaks to either side of the 8 eV VUV maximum then correspond to 5^1B_2 and 6^1B_2. It was impractical to compute more than 15 roots in SAC-CI for each irreducible representation owing to facility limitations. The group of relatively intense VUV peaks calculated circa 10 eV is probably too high in energy and relate to the observed band between 8.74 and 9.08 eV.

C. Ground state vibrational frequencies

The results from a resonance Raman (RR) study[28] of azulene-H_8 and azulene-D_8 are widely used, after minor corrections,[50] to provide the ground state fundamentals. These give a close correlation with the present X^1A_1 results at the CAM-B3LYP level. After re-designation of b_1 and b_2 vibrations, we find $\nu_{calc} = 1.056(9)\nu_{RR} - 15(14)$ cm^{-1}; the correlation coefficient (CC) is 0.997, and the standard errors (SE) are in parentheses. This correlation line lies very close to the origin, since its intercept is only slightly larger than its SE. These ground state frequencies are similar to both the experimental values[28,52] and DFT theoretical ones,[50,51] and are shown in the supplementary material as SM3.

D. Singlet excited state structures

A comparison between the microwave study[15,16] of the azulene X^1A_1 molecular structure, and that from our largest basis set, Def2TZVP, is shown in the supplementary material as SM4. Equilibrium structures, followed by vibrational frequency determinations, were obtained for several low-lying singlet states, including 1^1A_1, 2^1A_1, 1^1B_2, 2^1B_2, 1^1A_2, 2^1A_2, 1^1B_1, and 2^1B_1. These were obtained by use of the TDDFT procedure, where the symmetry and root of interest are user selected. The vibrational structure for these states is discussed below. As expected for a rigid molecular system, the variations with structure are relatively small; most bonds vary by less than 0.07 Å and most angles by less than 4°. The C_9C_{10} bond is typical, varying from 1.392 to 1.508 Å. Further details of the actual structures are given in the supplementary material as SM5.

E. Comparison of the theoretical absorption manifold of azulene with experiment

The harmonic frequencies for the 1^1B_2 state at 1.817 eV, using the CAM-B3LYP method with the 6-311G(d,p) basis set, is shown in Table II. The systematic nomenclature for vibrational spectroscopy has mode sequence numbers, $a_1 < a_2 < b_1 < b_2$, and is high to low frequency in each representation. G-16, including the Pisa software,[62–64] labels modes in ascending frequency rather than the

TABLE II. The harmonic frequencies (cm^{-1}) for the lowest excited (1^1B_2) state, determined by single excitation CI. The sequence numbers 1–48 apply for the vibrations excited by FC and/or HT processes.

1	2	3	4	5	6
$32b_1$	$23a_2$	$31b_1$	$48b_2$	$17a_1$	$22a_2$
120	194	286	338	394	407
7	8	9	10	11	12
$30b_1$	$47b_2$	$29b_1$	$16a_1$	$28b_1$	$21a_2$
510	512	582	686	691	708
13	14	15	16	17	18
$27b_1$	$20a_2$	$46b_2$	$26b_1$	$19a_2$	$15a_1$
741	771	781	823	881	887
19	20	21	22	23	24
$25b_1$	$14a_1$	$13a_1$	$24b_1$	$18a_2$	$45b_2$
905	927	957	996	1003	1055
25	26	27	28	29	30
$44b_2$	$12a_1$	$43b_2$	$11a_1$	$42b_2$	$10a_1$
1100	1102	1185	1251	1254	1268
31	32	33	34	35	36
$41b_2$	$40b_2$	$39b_2$	$9a_1$	$38b_2$	$8a_1$
1286	1371	1421	1453	1480	1500
37	38	39	40	41	42
$37b_2$	$7a_1$	$6a_1$	$36b_2$	$5a_1$	$35b_2$
1571	1619	1643	1925	3156	3160
43	44	45	46	47	48
$4a_1$	$34b_2$	$3a_1$	$2a_1$	$33b_2$	$1a_1$
3189	3191	3201	3227	3231	3262

spectroscopic sequence above; for simplicity, both sets of labels are shown in Table II. This binary system of labels applies to all other calculated vibrational states described below. All vibrational modes are in cm^{-1}, while intensity units are molar absorption coefficient ($dm.^3\ mol^{-1}.cm^{-1}$). All vibrational states with up to eight simultaneous excitations are included in our calculations. Many of these states have low intensity, but their considerable number (>10^5) allow these to make a significant contribution to the overall intensity.

Similarity of the vibrational frequencies for $S_2 \rightarrow S_1$ fluorescence with those from the $S_0 \rightarrow S_1$ absorption for azulene in a naphthalene mixed crystal at 4.2 K[33] led Gillispie and Lim to assignments for their a_1 and b_2 frequencies. A comparison of the present calculated data in Table II, over 20 (a_1 + b_2) vibrations, yields a linear correlation $\nu_{CAM\text{-}B3LYP}$ = 1.044 (14)$\nu_{Gillispie}$ −3.2 (168) cm^{-1}, with standard errors (SE) in parentheses and a correlation coefficient (CC) of 0.996; a similar correlation is found for comparison of our results with other studies.[73,77] These correlations give confidence that the present harmonic frequencies are close to the experimental results.

1. The lowest singlet state (1^1B_2, S_1) at 1.817 eV

We describe this state, in detail since this explains our approach. Solution spectra of azulene show four peaks in the 700–500 nm range, with separations of ~750 cm^{-1}. The highest resolution spectra for this state are in two jet-cooled studies using either two-color double resonance spectroscopy[24] or a cavity ring-down (CRD) absorption spectrum.[25] Both groups[24,25] propose spectral analyses that include symmetric and non-symmetric vibrations.[73,74] A comparison of our onset with the CRD spectrum, in the supplementary material as SM1, shows that the principal features are reproduced in both spectra. However, it appears that Fig. 1 of Suzuki *et al.*[24] with energy axis labeled wavenumber is non-linear and should correctly be labeled wavelength; for example, 14 500 cm^{-1} should be 145 nm. This scale change yields good agreement between Fig. 1 of both Suzuki *et al.*[24] and Ruth *et al.*[25] with the present study.

The color of azulene allowed its absorption and emission spectra to be determined as a very dilute solid solution in the host naphthalene at 20 K by Sidman and McClure (S & M).[22,23] Using earlier gas phase data,[75] they estimated the shift of the 0–0 band as 703 cm^{-1} to the red on solid solution formation; we found a slightly smaller shift of 633 cm^{-1} would correlate the S & M and present spectral results. The S & M absorption spectrum leads to a much more detailed picture than that generated by conventional methods.[75] This is reproduced in Fig. 3, where the baseline has been flattened by subtraction of a sigmoid function from the reported[23] signal in their Fig. 1. It is strongly polarized across the transverse-axis. Many of the spectral peaks in Fig. 3 are doublets, which become closer and merge as the energy increases. S & M suggest that the sharpness and polarization of the spectra indicate that azulene molecules occupy two lattice positions with almost identical environments in the naphthalene unit cell. An alternative assignment for the jet-cooled azulene spectra by Suzuki *et al.*[24] and Ruth *et al.*[25] for the $S_0 \rightarrow S_1$ for azulene, is included in the supplementary material (Table SM1).

Our TDDFT calculated 1^1B_2 state using the CAM-B3LYP functional is a $\pi\pi^*$-excitation with two leading configurations, as shown in Eq. (1). The FC profile is superimposed on the S & M spectrum in Fig. 3. Our calculated 0-0 band onset is at 16 773 cm^{-1} [excitation energy 2.358 eV, with f(r) 0.0117]. The observed band origin is at 14 652 cm^{-1} (1.817 eV),[23,26] and our profile has been shifted to 0–0 superposition.

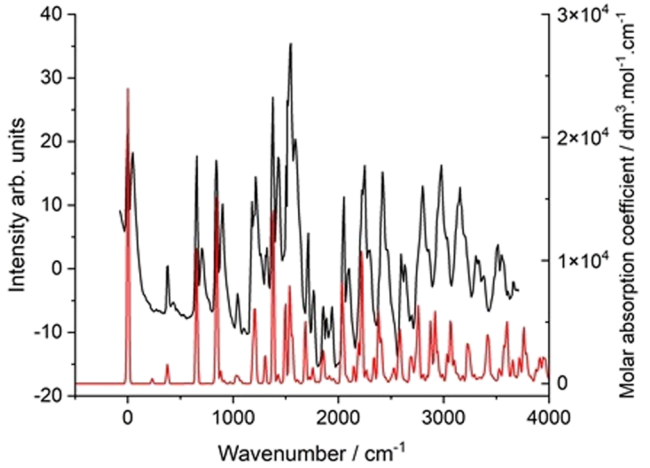

FIG. 3. The Sidman and McClure (S & M) onset band at 14 652 cm^{-1} after flattening of the baseline by subtraction of a best fit sigmoid function (black curve); the peaks in red are the Franck–Condon profile for this band, as described in the text. These have been aligned for the 0-0 bands to the lowest S & M peak; the alternative to the higher origin of S & M is equally possible and leads to little change in correlation.

S & M[23] identified three symmetric (a_1) frequencies, 384, 664, and 857 cm^{-1}, for this state; these clearly correlate with the three lowest a_1 vibrations of the present study at 394, 686, and 886 cm^{-1}, since there are no other a_1 modes close to these values. Their higher a_1 bands[23] at 1191, 1386, and 1554 cm^{-1}, correlate with our 1251 ($11a_1$), 1453 ($9a_1$), and 1619 cm^{-1} ($7a_1$) values. These six pairs of data lead to a linear correlation: $\nu_{CAM\text{-}B3LYP} = 1.053(61)^* \nu_{Sidman} - 11.1\ (6)$, with a CC of 0.999 83 and SE in parentheses. Thus, the calculated frequencies are 5.3% high, with a very low intercept (i.e., correction) of only 11.1 cm^{-1}. These corrections were then applied to all calculated Franck–Condon (FC) and Hertzberg–Teller (HT) data for this state, enabling the calculated profiles to be superimposed on the spectrum.

The FC profile (Table III) of this band shows that many a_1 fundamental modes and binary combinations are excited but with the 0–0 band having by far the highest intensity. The C–H stretching frequencies have negligible intensity. Those shown in Table III are where modes $5(17a_1)$, $10(16a_1)$, and $18(15a_1)$ are prominent. A set of vibrational states showing the range of vibrational types occurring close to the onset is shown in the supplementary material as SM6.

The HT vibrational states calculated for the 1^1B_2 band have intensities ~20 times weaker than the FC states and hence will have little impact on the profile of the combined set when compared with experiment; these are shown in Table IV. The calculated onset shows several non-symmetric modes with even quanta and relatively high intensity.

2. The singlet state (1^1A_1, S_2) at 3.478 eV

This excited state has band origin at 28 050 cm^{-1} (3.478 eV), and is polarized along the long z-axis, according to S & M.[23] Their

TABLE III. A selection of the most intense vibrational states, especially fundamentals, from the Franck–Condon profile of the lowest excited (1^1B_2) singlet state, determined by the CAM-B3LYP method with the 6-311G(d,p) basis set. The calculated 0–0 transition is at 16 770 cm^{-1}. Intensity units are molar absorption coefficient (dm^3 mol^{-1} cm^{-1}).

Position (cm^{-1})	Intensity	Vibration	Fundamental
0	2995	0^0	
394	187	5^1	17
686	1077	10^1	16
887	1363	18^1	15
927	80	20^1	14
957	20	21^1	13
1080	79	$10^1 5^1$	
1102	59	26^1	12
1251	331	28^1	11
1268	631	30^1	10
1281	128	$18^1 5^1$	
1372	270	10^2	
1453	1897	34^1	9
1500	73	36^1	8
1573	717	$18^1;10^1$	
1613	53	$20^1;10^1$	
1619	928	38^1	7
1643	408	39^1	6
3156	2.4	41^1	5
3189	0.6	43^1	4
3201	2.3	45^1	3
3227	0.9	46^1	2
3262	1.6	48^1	1

observed frequencies from this absorption band differed significantly from the onset S_1 absorption, and a series of possible assignments were offered in FC terms (i.e., only a_1 vibrations), which are discussed below.[23] The harmonic frequencies for the 1^1A_1 state, the generally assumed assignment, are shown in Table V; C–H stretching frequencies are excluded from later discussion; none appear to contribute. We will see that the S & M frequencies do not match with the calculated values in Tables VI and VII. The similarity between the rotational constants for the S_2 and S_0 states by microwave spectroscopy indicates that S_2 has an equilibrium structure similar to that of the ground electronic state.[76] This indicates that our calculated frequencies should be accurate. Our UV–vis spectrum for S_2 in this region, shown in Fig. 2, is a higher resolution version of the absorption in 3-methylpentane solution at 77 K.[41] However, it shows only a general similarity to the 28 050 cm^{-1} band of S & M, with considerable differences in groupings and balance. It appears that the polarized ultraviolet absorption system of azulene in naphthalene shown by S & M (their Fig. 3) is not directly comparable to the gas phase UV spectrum.

We compare our FC and HT data in Fig. 4, after subtraction of a ramp to flatten the axes of the experiment to enable comparison. The FC data in Table VI show an onset that is dominated by the 0^0

TABLE IV. The complete onset vibrational states from the Herzberg–Teller profile of the lowest excited (1^1B_2) singlet state, determined by the CAM-B3LYP method with the 6-311G(d,p) basis set. The calculated 0-0 transition is at 16 770 cm^{-1}. Intensity units are the molar absorption coefficient (dm^3 mol^{-1} cm^{-1}).

Position (cm^{-1})	Intensity	Vibration	Position (cm^{-1})	Intensity	Vibration
0	121.4	0	927	0.9	$10^1 1^2$
241	2.1	1^2	965	0.4	$14^1 2^1$
338	4.7	4^1	1020	0.6	7^2
388	0.3	2^2	1025	2.3	$10^1 4^1$
394	7.7	5^1	1055	0.7	24^1
512	13.7	8^1	1080	4.0	$10^1 5^1$
686	53.4	10^1	1100	27.5	25^1
708	3.4	12^1	1102	4.3	26^1
733	0.3	$5^1 4^1$	1128	1.1	$18^1 1^2$
752	0.4	$8^1 1^2$	1176	0.3	$15^1 5^1$
771	0.8	14^1	1185	2.7	27^1
781	6.6	15^1	1198	7.6	$10^1 8^1$
881	1.6	17^1	1225	3.1	$18^1 4^1$
887	66.0	18^1	1251	27.2	28^1
906	1.3	$8^1 5^1$	1254	19.1	29^1
927	0.5	20^1	1268	56.8	30^1

TABLE V. The harmonic frequencies (cm^{-1}) for the 1^1A_1 state, determined by single excitation CI. The sequence numbers 1–48 apply for the vibrations excited by FC and/or HT processes.

1	2	3	4	5	6
$32b_1$	$23a_2$	$31b_1$	$48b_2$	$22a_2$	$17a_1$
144	146	301	335	351	390
7	8	9	10	11	12
$47b_2$	$30b_1$	$29b_1$	$28b_1$	$21a_2$	$16a_1$
495	530	545	675	679	688
13	14	15	16	17	18
$27b_1$	$46b_2$	$20a_2$	$19a_2$	$15a_1$	$26b_1$
738	747	750	824	853	891
19	20	21	22	23	24
$14a_1$	$18a_2$	$24b_1$	$13a_1$	$25b_1$	$12a_1$
918	922	922	957	971	1017
25	26	27	28	29	30
$45b_2$	$44b_2$	$11a_1$	$43b_2$	$42b_2$	$10a_1$
1057	1072	1172	1175	1233	1254
31	32	33	34	35	36
$41b_2$	$9a_1$	$40b_2$	$39b_2$	$8a_1$	$38b_2$
1270	1349	1373	1421	1428	1458
37	38	39	40	41	42
$37b_2$	$7a_1$	$6a_1$	$36b_2$	$5a_1$	$35b_2$
1484	1595	1564	1614	3164	3172
43	44	45	46	47	48
$4a_1$	$34b_2$	$3a_1$	$2a_1$	$33b_2$	$1a_1$
3176	3191	3199	3251	3246	3255

TABLE VI. The calculated Franck–Condon onset to the S_2 state (1^1A_1), determined by the CAM-B3LYP method with the 6-311G(d,p) basis set. Energy of the 0–0 transition is 29 430 cm^{-1}. Intensity units are the molar absorption coefficient (dm^3 mol^{-1} cm^{-1}).

Position (cm^{-1})	Intensity	Vibration and quanta	Position (cm^{-1})	Intensity	Vibration and quanta
0	27 570	0^0	846	11	$9^1 3^1$
287	92	1^2	853	967	17^1
292	45	2^2	918	30	19^1
390	293	6^1	957	946	22^1
444	42	$3^1 1^1$	970	5	$16^1 2^1$
497	2	$5^1 2^1$	975	18	$12^1 1^2$
574	1	1^4	980	9	$12^1 2^2$
601	13	3^2	1018	28	24^1
670	1	4^2	1541	166	$17^1 12^1$
674	21	$8^1 1^1$	1645	180	$22^1 12^1$
677	1	$6^1 1^2$	1860	173	$27^1 12^1$
688	5 507	12^1	2281	143	$35^1 17^1$
703	124	5^2	2385	129	$35^1 22^1$
779	7	6^2	2521	138	$32^1 27^1$
819	2	$10^1 1^1$	2600	111	$35^1 27^1$
825	66	$11^1 2^1$	2843	135	34^2
831	6	$8^1 3^1$	2856	117	35^2

band; this profile cannot provide an explanation for the UV spectrum. The HT profile contrasts with the FC one in almost all details, through a wide range of fundamentals, overtones and combination bands having high intensity in the HT profile, while the 0^0 band is weak. Comparison of the combined FC + HT theoretical values with the observed spectra is an improvement on either separately. The comparison is far from ideal, since the balance of intensities is poor around the principal doublet close to 30 000 cm^{-1}, and there is insufficient intensity in the spectral tail. However, S_2 clearly differs greatly from S_1, in its FC and HT balance.

Returning to the S & M analysis of S_2, we find considerable similarity with many of their a_1 proposed assignments, but not all, since too many were proposed. Our descending sequence of 11 a_1 symmetry members, from 1581 to 408 cm^{-1}, is to be compared with their 14 members from 1568 to 336 cm^{-1}. The higher frequency members are well spaced in both series and a correlation seems clear. The relation between the a_1 fundamentals for the 1^1A_1 state is ν_{Calc} = 0.986 (26) $\nu_{S\&M}$ + 67 (28) cm^{-1}, with a CC of 0.993, and SD in parentheses. When this correlation is extended to the lower frequencies, then it is clear that the S & M values 336, 804, and 856 cm^{-1} do not fit, and hence the tentative assignment of these as a_1 fundamentals is unlikely.

In the discussion of the higher singlet states of azulene, the pattern of tables is similar to the above for the two lowest states. For brevity, most of these higher singlet state tables have been transferred to the supplementary material.

3. The S_3 singlet state (2^1B_2) at 4.219 eV

It has been claimed that this region has never been satisfactorily explained.[40] Most of the intensity of this region is the rise of the strongest S_4 band at higher energy. The calculated profile of S_4 shows a very intense 0–0 band; minor undulations on the leading edge of S_4 in Fig. 2 do not give the appearance of hot-bands for S_4. We separate these minor peaks from the rise of S_4 by subtracting a 7th order polynomial, the lowest power to give a close fit to the S_4 spectrum; the resultant regular residuals are shown in Fig. 5.

The FC envelope for S_3, shown in the supplementary material (Table SM7), using ascending frequency listing, demonstrates that the calculated 0–0 band is dominant, but fundamentals, 7^1, 13^1, 20^1, 22^1, and 25^1, have relatively high intensities. However, the state shows numerous vibrational states where the non-symmetric fundamental is raised to even numbers of quanta; examples of overtones are 4^2 and 6^2; similar binary and higher combination bands (such as $6^1 2^1$) also occur.

The 0^0 band of the HT onset, as shown in the supplementary material (Table SM8), is 30 times less intense than that of the FC profile. Non-symmetric modes occur widely. The most intense vibrational band in the HT profile is the fundamental 32^1. We conclude that S_3 is narrow as a result of domination by low-frequency modes both in the FC and HT models.

The structure above 4.39 eV in Fig. 5 is similar to the IE_1 ionic state shown in mangenta,[7] leading to assignment as a Rydberg state. McGlynn *et al.*[39,40] previously suggested that the lowest-energy *p*-Rydberg $2a_2 3p$ transitions must occur in the vicinity of S_3. A further member of the 3p set may occur on the side of the principal $\pi\pi^*$ absorption as shown in the blue curve. These bands close to 36 000 cm^{-1} disappear in solution,[41] another indication of their Rydberg state character. Higher Rydberg states, lying in the range 51 000–47 000cm^{-1} (5.703–6.623 eV), show this same profile.[39]

TABLE VII. The calculated Herzberg–Teller fundamentals for the S_2 state (1^1A_1), determined by the CAM-B3LYP method with the 6-311G(d,p) basis set. Energy of the 0–0 transition: 29 431 cm^{-1}. Intensity units are the molar absorption coefficient ($dm^3\ mol^{-1}\ cm^{-1}$).

Position (cm^{-1})	Intensity	Vibration and quanta	Position (cm^{-1})	Intensity	Vibration and quanta
0	536	0^0	1175	730	28^1
144	5	1^1	1183	43	12^17^1
287	2	1^2	1233	3 054	29^1
301	7	3^1	1233	87	12^19^1
335	15	4^1	1242	462	17^16^1
390	3 578	6^1	1254	2 417	30^1
495	219	7^1	1270	901	31^1
530	5	8^1	1305	264	24^11^2
545	437	9^1	1310	82	24^12^2
688	68	12^1	1346	138	22^16^1
738	110	13^1	1349	20 260	32^1
747	433	14^1	1373	2 022	33^1
779	93	6^2	1407	409	24^16^1
853	5 492	17^1	1421	169	34^1
891	56	18^1	1458	2 394	36^1
918	80	19^1	1459	161	27^11^2
922	421	20^1	1495	2 536	38^1
957	52	22^1	1541	1 052	17^112^1
971	405	23^1	1561	1 080	27^16^1
1018	54 320	24^1	1564	1 354	39^1
1057	15	25^1	1614	1 671	40^1
1072	2 285	26^1	1706	491	17^2
1172	32 320	27^1	1706	10 840	24^112^1

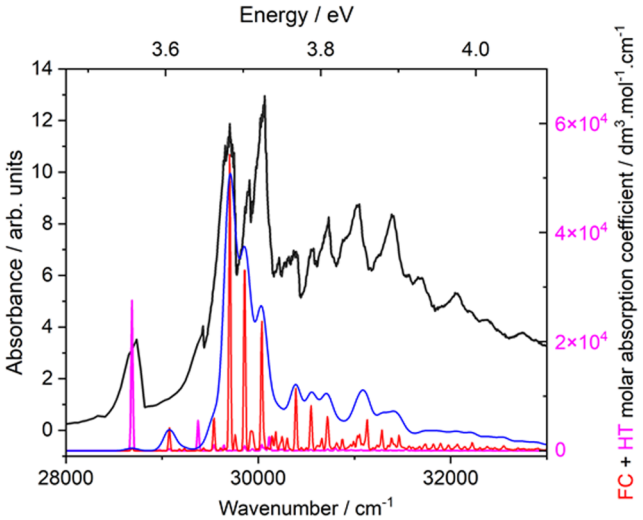

FIG. 4. The S_2 state (1^1A_1 in black) after subtraction of a ramp to give a horizontal axis. The Franck–Condon (magenta) and Herzberg–Teller (red and blue) profiles are shown where the half widths at half maximum are 10 (red) and 70 (blue) cm^{-1}. No scaling of the results for best fit has been performed.

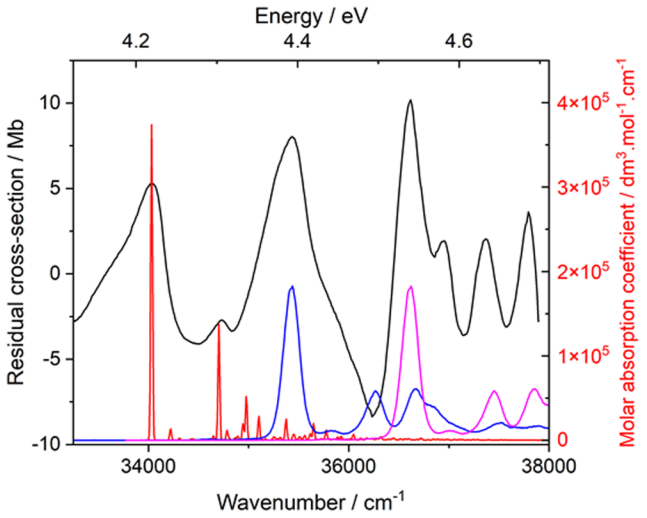

FIG. 5. The S_3 band and calculated FC profile (in red) together with structure of two Rydberg states (in blue and magenta) at higher energy, as discussed in the text.

4. The S_4 singlet state (2^1A_1) with peak maximum at 4.700 eV

This is the most intense absorption by far. Its overlap with the tail of the very weak S_3 (2^1B_2) band discussed earlier, is clearly demonstrated in Fig. 6. A list of the principal vibrational states for S_4, shown in the supplementary material (Tables SM9–SM11), is relatively simple. Since the theoretical calculations for both S_3 and S_4 are performed independently, interaction between them is impossible, and thus the calculations represent the unperturbed bands. The FC

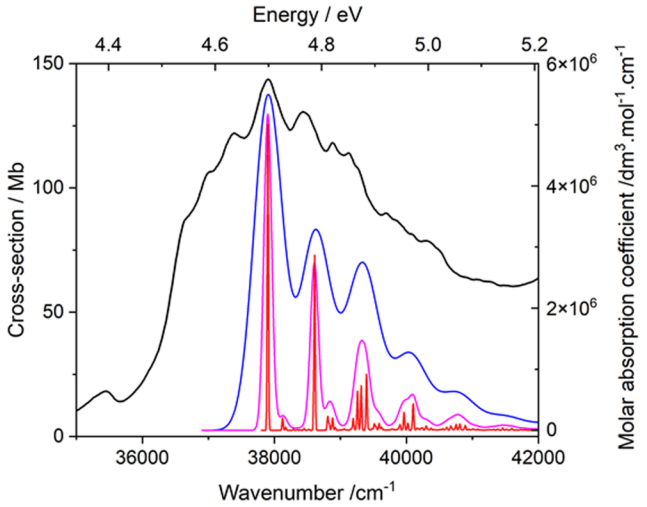

FIG. 6. The principal maximum of the azulene VUV spectrum, S_4, with the Franck–Condon profile superimposed. There is a very clear overlap with the preceding very weak S_3 state, and the weak sub-structure around 37 000 cm^{-1} is one or more Rydberg states rather than S_4, since the 0–0 band of S_4 is predicted to be the highest intensity of the band.

profile for S_4 is dominated by the 0-0 band and several fundamentals with frequencies below 1100 cm^{-1}. The HT profile has a very low 0-0 band but is also dominated by low frequency vibrations. The theoretical vibrational states for S_4 included in Fig. 6 are simulated by means of Gaussian functions with several band broadening functions, indicated by different colors. The sharpest peaks (shown in red) have Half-Widths at Half-Maximum (HWHM) of 10 cm^{-1}, with those in magenta (70 cm^{-1}, which are usually suitable to reproduce the width of an isolated vibrational peak), and 250 cm^{-1} (in blue). Taken together, these show consolidation of several vibrational states into broad maxima. Even that largest HWHM is insufficient to account for the small local bands observed; we have previously shown that when two (ionic) states overlap in this way, the necessary HWHM to account for the width observed can be 400 cm^{-1} or more. Similar considerations occur here.

Both Blanchet *et al.*[44] and Lewis *et al.*[40] assign a 3px Rydberg state to the vicinity of the peak maximum for S_4; this RS has binding energy (BE) ~2.69 eV and hence electronic energy (EE) 4.72 eV. Although close to the peak maximum, S_4 is clearly not an RS; its high calculated oscillator strength and spectral cross section make this impossible. The MPI methods used[40,44] must focus upon either a close or underlying weak band. Their pump probe at 4.626 eV (268 nm) lies very close to the VUV absorption maximum. A 2nd Blanchet *et al.*[44] MPI RS, with BE 2.22 eV and hence EE 5.19 eV, was correlated with a state having BE 2.16 eV and EE 5.15 eV previously assigned to a 3p-RS by Kuthirummal and Weber in a further MPI study.[43] That work is supported by the observation of several RS with PQN 3 or 4, and, in particular, the twin *n*d series of Kitagawa *et al.*[37]

5. The S_5 singlet state (3^1B_2)

This has been reported to lie on the tail of S_4 at 5.166 eV.[19] Mann *et al.*[46] compared the UV + VUV spectra of azulene with naphthalene; their 4th band with onset 40 300 cm^{-1} and peak maximum at 42 300 cm^{-1}, is featureless; this is our 5th band, since S_3 was not observed by them. This 5th calculated singlet state is 3^1B_2 using the CAM-B3LYP functional in the TDDFT method. Since its oscillator strength is 0.251, it is expected to make a significant contribution to the experimental cross section. The structure of S_4 and its theoretical interpretation are shown in Fig. 6; we believe that the profile for S_4 is basically complete by 5.2 eV, and that absorption to higher energy/wavenumber must be either S_5 and/or Rydberg in nature.

The VUV spectrum from 5.08 to 5.70 eV shows a nearly linear decline in cross section with increasing energy, but with several relatively weak peaks superimposed. Subtraction of a ramp from the cross section then leads to Fig. 7. The first main peak at 5.231 eV is very close to the 3p state identified by Kuthirummal and Weber.[43] Our spectrum in Fig. 7 is much more complex and does not present the profile of one or more Rydberg states.

F. The spectral Rydberg states of azulene

These have been reported by several groups, especially in the energy region 5.579–7.439 eV;[37,38,40,41] two RS series were successfully extrapolated to yield a relatively accurate value for the IE_1 for azulene. The two lowest ionization energies for azulene are 7.409 (X^2A_2) and 8.598 eV(A^2B_1), an energy difference between IE_1 and

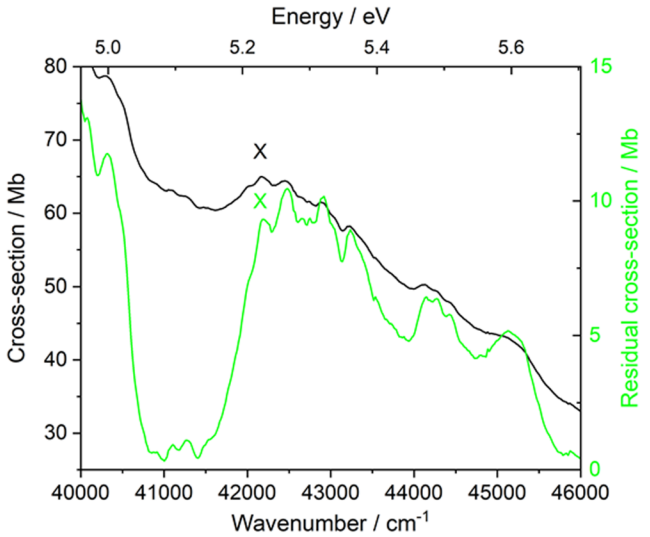

FIG. 7. The 41 000–46 000 cm^{-1} region of the VUV spectrum of azulene, after flattening of the sloping baseline to horizontal, by removal of a ramp. The first main peak marked X, at 5.231 eV, is very close to the 3p state identified by Ref. 43.

IE_2 of 1.189 eV. Profiles of the X^2A_2 and A^2B_1 ionic states are compared in the supplementary material as SM12; both are dominated by 0-0 bands, with relatively similar vibronic structure. This makes RS identification based on IE_2 difficult, and currently no such states have been claimed. The adiabatic IE_3 for B^2A_2 at 9.93 eV is well defined, but the main structure of the band is complex; this is a result of many overlapping low frequency vibrations. There is currently no prospect of identifying RS leading to IE_3 for that reason.

The relationship between the RS energy (E_n) and the ionization energy is shown in Eq. (2); other terms are the principal quantum numbers (PQN, *n*) and quantum defect (δ). Conventional values for δ are ~0.9 (s-states), ~0.3–0.6 (p-states), ~0.1 (d-states), and ~0.0 (f-states), while the PQN start at 1s, 2p, 3d, and 4f.[17,18]

The relationship between ionization energy (IE) and Rydberg state energy (E_n) is as follows:

$$E_n = IE - 13.61/(n-\delta)^2. \quad (2)$$

As noted above, IE_1 for azulene has leading configuration $2a_2^{-1}$, and $2a_2ns$ Rydberg states are optically forbidden;[40] Robin[17,18] reassigned earlier $2a_2ns$ results,[37,38,40,41] to $2a_2nd$, where δ = −0.09 or −0.12, respectively. Negative quantum defects had already been proposed for the naphthalene *n*d series.[17] The detailed symmetry in C_{2v} for these d-type states has not been reported, and the question of whether the lowest observed are 3d or 4d is also unanswered to date.

McGlynn *et al.*[46,47] studied azulene absorption from 5.951 eV to 11.271. Their results[40,41] for two series "A" and "B" in the 5.951–7.438 eV region are very similar to those of Kitagawa,[37] but measured to higher precision. These gave effective (i.e., non-integral) principal quantum numbers (EPQN, *n*-δ) from 3.10 to 8.83. If their measured peaks are simultaneously fitted to the Rydberg

equation, we find that the extrapolated IE_1 and δ are effectively identical with A-series [7.404(2) and −0.111(5)] and B-series [7.415(9) and −0.117 (17)], respectively. Lack of vibrational structure at the high energy end of the range, potentially leading to IE_2 (A^2B_1), was ascribed[40,41] to autoionization followed by collapse to IE_1. Super-excited state MPI processes[26] have added to the overall RS information; three RS with $n = 4$ were obtained with δ = 0.57, 0.41 and 0.23; these are presumably two 4p-states and a 4d-state. Although similar values were obtained for naphthalene, the spectral profiles are quite different.[42] Results obtained by these MPI methods have been assessed by Blanchet *et al.*,[44] and are discussed below in relation to our calculated RS.

The overall profile of our Rydberg state region shows a marked increase in signal to noise than previous studies, and is shown in the supplementary material as SM13. We have electronically fitted 36 of the peaks in this spectrum, using the "peak-pick" method in Origin (2021b); the peak energies [E(x) in eV] and relative intensities (Mb) are shown in the supplementary material as SM14. Although our VUV spectrum does not show major new features, when compared with earlier spectra, the very high cross section and the electronically measured peak positions make the Rydberg state features much higher in intensity than surrounding noise and allow magnification, as in Figs. 4–7, to be more reliable.

As expected, portions of the profiles for VUV absorption and photoionization for azulene are very similar;[40,41] the VUV spectral RS yielded three vibrations, 440, 849, and 1230 cm^{-1}, which were compared with 4 vibrations, 830, 1130, 1340, and 1990 cm^{-1} (all ±70 cm^{-1}), in early PES of azulene.[77] Our recent re-analysis[7] of the azulene PES concluded that the two main vibrational peaks above the 0-0 band are actually doublets, 410 and 696 cm^{-1} (modes 6^1 and 10^1, respectively), and 859 and 911 cm^{-1} (modes 15^1 and 17^1), respectively; a higher vibration occurred at 1275 cm^{-1} (mode 30^1). Thus, the frequencies given by these early studies are (accidentally) relatively close to our current values.

We now consider separate regions of the VUV spectrum, especially in light of our calculated Rydberg state energies. The energy region above S_4 is more complex than the theoretical profile presented in Fig. 6. The VUV region from 37 000 to 42 000 cm^{-1} is shown in Fig. 8, with the leading part of the PES shifted to lower energy to best fit the VUV profile of a RS. In order to fit the leading doublet of the PES to the VUV profile, it is necessary to shift the PES peak maximum to 38 033 cm^{-1} rather than to the maximum of the VUV at 37 902, a difference of 131 cm^{-1}. Blanchet *et al.*[44] give 38 070 cm^{-1} and Lewis *et al.*[41] give 37 989 cm^{-1} for a 3px-RS, and these are clearly identical to the assignment shown in Fig. 8; this is the first assignment of a 3p-RS from a VUV spectrum.

The peak X between A and B in Fig. 8, could be part of the S_4 structure described earlier, and it certainly does not correlate with any of the RS collected in Blanchet *et al.*,[44] since its apparent BE is 2.605 eV. However, using our A^2B_1 state energy 8.598 eV, this BE would give $n - \delta = 2.286$ eV, and hence a realistic value for a 3s RS based on IE_2 with δ = 0.714; we believe this conclusion is correct.

There remain several state binding energies listed by Blanchet *et al.*[44] where future assignments are awaited. These include apparently significant differences occurring in measured BE between alternative authors for the same state; also, 4s RS levels apparently leading to X^2A_2 are given, which appear to be FC forbidden.

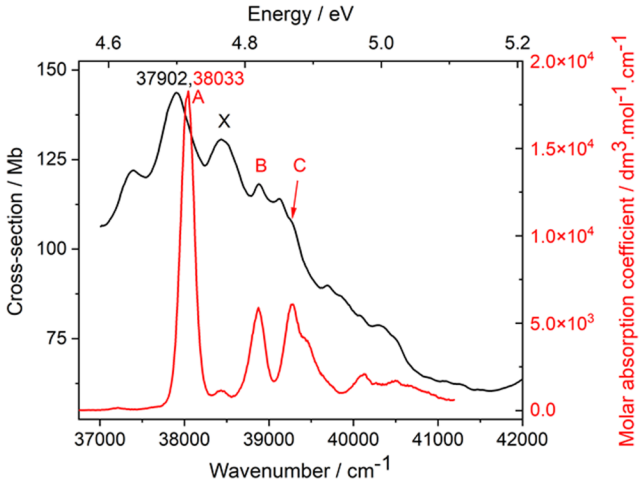

FIG. 8. The 37 000–42 000 cm^{-1} region of the VUV spectrum of azulene, where the leading profile of the X^2A_2 state (peaks A, B, and C) of the photoelectron spectrum, after a shift to lower energy by 21 722 cm^{-1} (2.6931 eV), has been superimposed in red. The two peak maxima of the PES and VUV shown are separated by 131 cm^{-1} to allow for better alignment of the leading doublet B + C.

G. Calculated Rydberg state energies

Using the MRD-CI method,[70,71] identification of the leading configurations as either valence or Rydberg is immediately obvious from the second moments of the charge distribution (SECMOM); examples are shown in the supplementary material as SM15. The orbital energies of the very diffuse GTOs representing Rydberg functions lie immediately above the zero energy level, i.e., at positive energy, but much closer to zero than the valence virtual orbitals (VMOs). At the CI level, valence states (VS) often lie within the calculated energy range for the n = 3–5 lowest RS. These VS behave as intruder states; that is, the states have the desired symmetry, but incorrect leading configurations. When close to a calculated RS, they perturb it, and potentially lead to linear combinations of VS ± RS, since all belong to the same irreducible representation. Here we note that in MRD-CI the full CI matrix is separated into separate submatrices of $^1A_1$, $^1B_1$, $^1B_2$, and $^1A_2$ symmetry. These include both occupied and virtual orbitals so that the VS and RS have sequential root numbers. Thus, the a_1 doubly occupied MOs (DOMOs) have sequence numbers 1–11, and the s-Rydberg orbitals, also of a_1 symmetry, follow immediately with sequence numbers 12, 13, and 14. Each electronic state is described by one or more configuration state functions (CSFs), as shown in Eq. (1).

The principal RS results using either the TDDFT method with the CAM-B3LYP functional, or the MRD-CI method at the Hartree–Fock level, are shown in the supplementary material (Table SM16). Rydberg states and their ionic limits share a common vibrational envelope, implying that their structures are similar, at least to first order. The RS in MRD-CI behave as a group, since the same set of reference configurations are diagonalized simultaneously to generate the set of roots with their vertical excitation energies (VEE). In TDDFT, because of the structural similarity of individual RS of

same symmetry, optimization of the lowest state generates its adiabatic excitation energy (AEE); the relative energies of higher RS of same symmetry are determined at the same time; these can also be treated as a group.

1. The optically forbidden theoretical ns-Rydberg states

The lowest IE, X^2A_2 is dominated by $2a_2^{-1}$, and presents the simplest situation relating to VS and RS interaction in VUV absorption. The TDDFT results fitted to the Rydberg state equation leads to AIE_{1A2} = 6.802 eV and δ = 0.309, with standard errors (SE) 0.4 or 9%; our previous IE_1 is 7.409 eV;[7] this is acceptable since extrapolation from calculated values for n = 3, 4 and 5 to infinity cannot be expected to be precise. The MRD-CI values offer additional flexibility when an intervening VS close to the RS with n = 5 is included or excluded; for (inclusive) IE_1 and its δ are 6.898 eV and 0.478 and 7.170 for the excluded value; the SE are at 2% and 24% in both cases. The intruder VS is $2a_2 17a_1{}^*$, which lies immediately above the three Rydberg VMOs in the orbital energy sequence.

The corresponding values for the excitation process $3b_1ns$ are also shown in the supplementary material (Table SM16); the higher energy of the states makes the effect of the corresponding intruder state $3b_1 17a_1{}^*$ less important. The extrapolated VIE_2 using the MRD-CI method are 8.144 (1%) and with δ 0.656 (9%) for the included intruder state, and 8.353 eV (2%) with δ 0.621 (23%) for the VS excluded state. These are to be compared with our recent PES study[7] of VIE_2 8.598(1) eV (A^2B_1). It is usual for CI estimations of IE to lie at lower energies than experiment, since there is an inability of the method to balance the degrees of electron correlation between the ground state (a relatively small number of CSF) with the excited (or ionized) state with a very much larger number of CSF. In the discussion above, it is uncertain whether any of these states have been observed experimentally in the UV + VUV spectrum. The TDDFT method predicts the 3s- and 3p-Rydberg state ($^1B_2$), shown in the supplementary material (Table SM15), with δ 0.740 (17) and 0.398 (21), respectively. Only two $2a_2$3p-states are allowed.

2. The calculated np-Rydberg states

Addition of a set of np-Rydberg functions to the 6-311G(d,p) basis set adds extra CI roots, with orbital symmetries a_1, b_1, and b_2, respectively. In most of our TDDFT studies using the CAM-B3LYP functional, the RS roots are preceded by the 4 lowest valence states in Eq. (1) as roots 1–4, respectively. Optimization of the next three Rydberg states leads to the adiabatic excitation energies: 1^1B_1 [5.287 eV with f(r) 0.0018], 1^1A_2 [5.291 eV, f(r) 0.0], and 3^1B_2 [5.518 eV, f(r) 0.0022]; these are 3py, 3pz, and 3px, respectively. Thus, the $2a_2$3py excitation lies at marginally lower energy than the other members of the group. Extrapolation of the three lowest RS member energies, shown in the supplementary material (Table SM16), gives the theoretical IE_1 of 7.172 eV (2.7%) with δ 0.338, but a higher SE uncertainty of 64%; however, these results are similar to the theoretical $2a_2ns$ $\pi\sigma^*$-excitation above. Here, SE are expressed as % errors rather than absolute errors. The $2a_2$3py excitations ($^1B_1$) again give reasonable values after extrapolation, giving IE_1 7.170 eV (2.7%) and δ 0.337 (64%). Finally, the $2a_2n$px series yield IE_1 7.246 eV, with a lower δ of 0.241.

3. The calculated nd- and nf-Rydberg states

Having noted that the symmetry of the previously reported $2a_2n$d-Rydberg series is currently unknown, we have calculated the energies of several of the lowest Rydberg states, concentrating on the nd-series. Processing of the nd- and nf-states in MRD-CI are routine, where we use the 6d- and 7f-cartezian versions of the spherical harmonics; these simplify the mixing with the C_{2v} state of the azulene carrier.

The lowest excited state of azulene, the 1^1B_2 state, is shown in Eq. (1). In order to generate $2a_2n$d states of $^1B_2$ symmetry from the input reference configurations, we needed to suppress the VS terms. The Rydberg basis set results in the lowest 1^1B_2 state being perturbed, to the higher excitation energy, 2.937 eV, compared with the unperturbed excitation energy of 2.358 eV discussed above. The following roots are 3d, 4d, and 5d-RS with energies 5.461, 6.119, and 6.926 eV. The projected IE_1 for this $^1B_2$ series is 7.388 eV (4.1%) with δ 0.380 (84.9%), where standard errors are in parentheses, to be compared with the PES IE_1 at 7.409 eV; this projection is close to experiment. Based on these calculated $2a_2n$d Rydberg states, we extrapolated to generate comparable data to the seven states (n = 3–8) observed by Bouler *et al.*[39] for azulene. The spacing is very close, but a graph (not shown) has a considerable slope and intercept. The correlation is $\nu_{Bouler} = 1.247\ \nu_{2a2nd} - 13\,967\ cm^{-1}$, with adjacent R^2 0.9984. The intercept may be an indicator that the Bouler *et al.*[39] data should have their EPQN as n = 3.10–9.83.

Two alternative determinations of the 3d, 4d, and 5d-RS were within the $^1B_1$ and $^1A_1$ manifolds; $^1B_1$ is simpler, since there are no low-lying VS of this symmetry. A fit of the calculated RS with values 5.489, 6.159, and 7.167 eV gives the projected IE_1 as 7.5936 eV (5%) and δ 0.501 (77%). The $^1A_1$ sequence has an intruder state as the leading (lowest energy) root, easily recognized from its high f(r) and low SECMOM relative to roots 2–4. The 3d, 4d, and 5d-RS have energies 5.473, 6.482, and 6.953 eV, which when fitted to the Rydberg equation give IE_1 7.599 (0.4%) and δ 0.473 6%); these values are slightly higher than the $^1B_1$ and $^1B_2$ nd states, but there is no requirement for degeneracy.

The simplest optically allowed f-Rydberg states are the $^1B_1$ series; but the lowest f-RS appears to be the $2a_2nf$ ($^1A_2$) series with n 4, 5, and 6, as shown in the supplementary material (Table SM16). The extrapolated IE_1 is 7.149 eV (5.8%), but the calculated δ is unexpectedly large at −0.449. These f-RS are particularly simple to calculate using MRD-CI, since the method is focused upon the desired symmetry only, and states of other symmetry are ignored.

IV. CONCLUSIONS

All of the calculated singlet valence states S_1 to S_4 have two leading configurations, the most prominent involve excitations from the two HOMOs to the two lowest LUMOs. All of these states are $\pi\pi^*$ rather than $\sigma\sigma^*$ excitations. Although the calculated $^1B_1$ states ($\pi\sigma^*$, $\sigma\pi^*$) have non-zero oscillator strengths, most are very weak; this leads to the VUV absorption spectrum being dominated by the $^1A_1$ and $^1B_2$ states. Generally, the valence portions of the spectrum are well represented by the energy profile generated from the high level coupled cluster (SACC-CI) calculations. The wide scan spectrum from 1.5 to 11 eV shows valence states at both the onset and high energy regions, but the mid-energy region is dominated by Rydberg states.

The present TDDFT level calculations allow the vibrational coupling within several of the singlet states to be evaluated using the Pisa Group software. The onset S_1 state of Sidman and McClure in Fig. 3 is closely reproduced by our calculations at the Franck–Condon level. However, some of the apparent doublets given are not identified by Herzberg–Teller study, and these may be a result of more than one crystal site for the solid solution spectra. The HT vibrations appearing in this 1^1B_2 band mostly have intensities ~20 times weaker than the FC states, and hence will have little impact on the profile of the combined set when compared with experiment. Many fundamental modes are excited, but with a very wide range of intensities. Numerous binary combinations occur, in which modes 5 ($17a_1$), 10 ($16a_1$), and 18 ($15a_1$) are prominent.

It appears that the polarized ultraviolet absorption system of S_2 azulene in naphthalene shown by S & M (their Fig. 3) is different from the gas phase UV spectrum. Our FC data show an onset, dominated by the 0^0 band, with little vibrational intensity from any of the fundamentals, overtones, or combination bands; this profile cannot provide an explanation for the S_2 spectrum. The situation is improved when the HT profile is included, since this contrasts with the FC one, with a wide range of fundamentals, overtones, and combination bands. The HT 0^0 band is weak, while ascending sequence modes 24 ($24b_1$), 27 ($11a_1$), and 32 ($9a_1$) are extremely intense. None of these are prominent in the FC profile. Combination of the FC + HT profiles, gives a closer match to the experimental spectrum in main groupings, but S_2 clearly differs greatly from S_1, in its FC and HT balance.

Most of its intensity for the S_3 state lies on the rise of the strongest S_4 band at higher energy. After removal of the slope associated with S_4, much of the residual structure above S_3 is similar to the IE_1 ionic state. This leads directly to assignment as Rydberg states, in agreement with earlier studies. We propose that two $2a_2 3p$ Rydberg state of the 3p set occur here. Much of the intensity of the VUV spectrum between 4.4 and 5.2 eV is the S_4 band, where we find that the FC profile provides a realistic interpretation. The energy region above S_4 is more complex than the theoretical profile presented in Fig. 6. In order to fit a PES profile for the 3px-Rydberg state in the VUV region from 37 000 to 42 000 cm^{-1}, it is necessary to place the PES peak maximum to 38 033 cm^{-1} rather than at the maximum of the VUV at 37 902, a difference of 131 cm^{-1}. Blanchet *et al.*[44] give 38 070 cm^{-1} and Lewis *et al.*[40] give 37 989 cm^{-1} for this Rydberg state but do not appear to differentiate the valence state maximum from the PES one.

The Rydberg state region of the VUV spectrum, between 5.75 and 7 eV, shows no additional information to that extracted by earlier workers, so that our principal contribution here lies in the theoretical RS determinations. We find that the use of very diffuse GTOs allows straightforward determination of s-, p-, d-, and f-RS, especially using the MRD-CI system within GAMESS-UK. The higher members of these states lie high up in the singlet state manifold. This makes the TDDFT method more difficult to use, since all 4 representations of C_{2v} are treated simultaneously; MRD-CI treats each representation separately. There is little comparison with the n = 3–8 nd-RS previously reported, since we can only cover the range n = 3–5; the extrapolated energies of these calculated states are generally close to our recent re-determination of the lowest X^2A_2 ionic state energy. The same procedure was applied to RS leading to the A^2B_1 state, where no experimental RS have yet been observed.

Extrapolation to infinity using Eq. (2) for the low-lying members of RS which have PQN 3–5; inevitably produces uncertainties in the values obtained. The standard errors for the IE, are generally small in absolute energy terms, and just a few percentage points; this is the principal reason for the projection. Errors for the quantum defect are markedly higher. An early graphical procedure for determining (n – δ) directly from three successive members of the RS, purely in terms of the energies of the three states has been given;[78] such a method should produce lower errors than our projection used here, but apparently generates other uncertainties,[78] and we were unable to exploit the principle.

SUPPLEMENTARY MATERIAL

See the supplementary material for additional information on each of the following:

The onset of the azulene UV spectrum, recorded using a Unicam UV340 spectrometer, compared with the multi-photon ionization spectrum of Suzuki *et al.*[24] (Fig. SM1). An alternative assignment for the jet-cooled azulene spectra by Suzuki *et al.* (Table SM1). (2) The full set of SACCI singlet state energy levels as depicted in Fig. 2, and state properties (Table SM2). (3) The harmonic frequencies for the X^1A_1 state of azulene (cm^{-1}) (Table SM3). (4) The azulene equilibrium structure at the Hartree–Fock level with the Def2-TZVPPD basis set (Fig. SM4). (5) The singlet state structures of azulene compared with the parent molecule using the CAM-B3LYP method with the 6-311G(d,p) basis set (Fig. SM5). (6) The full onset of vibrational states from the Franck–Condon profile of the lowest excited (1^1B_2) singlet state, determined by the CAM-B3LYP method with the 6-311G(d,p) basis set (Table SM6a). (7) The full onset of vibrational states from the Herzberg–Teller profile of the lowest excited (1^1B_2) singlet state, determined by the CAM-B3LYP method with the 6-311G(d,p) basis set (Table SM6b). The vibrational intensities contributed by the fundamentals to the Herzberg–Teller profile of the lowest excited (1^1B_2) singlet state, determined by the CAM-B3LYP method with the 6-311G(d,p) basis set (Table SM6c). (7) Table SM7. The calculated Franck–Condon fundamentals for the S_3 state (2^1B_2). (8) Table SM8. The calculated Herzberg–Teller fundamentals for the S_3 state (2^1B_2). (9) Table SM9. Harmonic frequencies for the S_4 state. (10). Table SM10. Principal fundamental and combination band vibrational states, at the Franck–Condon level, based on intensity, for S_4 in azulene, 2^1A_1 (11) Table SM11. The vibrational structure of the onset of the Herzberg–Teller structure to the 4th excited state (S4, 2^1A_1) state. (12) Profiles of the X^2A_2 and A^2B_1 lowest ionic states compared, by lowering the energy of the latter by 8735 cm^{-1} (Fig. SM12). (13). The principal Rydberg state region of the VUV spectrum of azulene between 42 000 and 61 000 cm^{-1} (Fig. SM13). (14) The peak energies, measured in wave-numbers with relative intensities (Mb) for the principal Rydberg state region of azulene between 46 000 and 61 000 cm^{-1} (Table SM14). (15) Dipole and second moments of the charge distribution (Table SM15). (16) Table SM16. The calculated Rydberg states for azulene using either the CAM-B3LYP functional under TDDFT, or Hartree–Fock with MRD-CI.

ACKNOWLEDGMENTS

We thank the ASTRID2 Synchrotron Facility and Aarhus University for a grant of beamtime, and the University of Edinburgh

(Eddie3) and Edinburgh Parallel Computing Center (Cirrus) for super-computing support. Numerical fitting was performed using Gnuplot-5.0.5;[79] plotting used Origin 7.0[80] and visualization used GaussView.[81]

AUTHOR DECLARATIONS

Conflict of Interest

The authors have no conflicts to disclose.

Author Contributions

Michael H. Palmer: Data curation (equal); Funding acquisition (equal); Methodology (equal); Software (equal); Supervision (equal); Validation (equal); Visualization (equal); Writing – original draft (equal). **Nykola C. Jones**: Investigation (equal); Methodology (equal); Project administration (equal). **Søren Vrønning Hoffmann**: Funding acquisition (equal); Investigation (equal); Project administration (equal); Resources (equal); Software (equal). **R. Alan Aitken**: Data curation (equal); Resources (equal). **Marcello Coreno**: Investigation (equal); Software (equal); Writing – review & editing (equal). **Monica de Simone**: Investigation (equal); Project administration (equal); Software (equal); Writing – review & editing (equal). **Cesare Grazioli**: Data curation (equal); Project administration (equal); Writing – review & editing (equal). **Iain L. J. Patterson**: Data curation (equal); Software (equal).

DATA AVAILABILITY

The data that support the findings of this study, including its supplementary material, will be available from the corresponding author upon reasonable request.

REFERENCES

[1] M. H. Palmer, M. Coreno, M. de Simone, C. Grazioli, S. V. Hoffmann, and N. C. Jones, J. Chem. Phys. **150**, 194305 (2019).
[2] M. H. Palmer, S. V. Hoffmann, N. C. Jones, M. Coreno, M. de Simone, and C. Grazioli, J. Chem. Phys. **151**, 084304 (2019).
[3] M. H. Palmer, R. A. Aitken, M. Coreno, M. de Simone, C. Grazioli, S. V. Hoffmann, and N. C. Jones, J. Chem. Phys. **152**, 144301 (2020).
[4] M. H. Palmer, S. V. Hoffmann, N. C. Jones, M. Coreno, M. de Simone, C. Grazioli, and R. A. Aitken, J. Chem. Phys. **153**, 054301 (2020).
[5] M. H. Palmer, M. Coreno, M. de Simone, C. Grazioli, R. A. Aitken, S. V. Hoffmann, N. C. Jones, and C. Peureux, J. Chem. Phys. **153**, 204303 (2020).
[6] M. H. Palmer, S. V. Hoffmann, N. C. Jones, M. Coreno, M. de Simone, C. Grazioli, and R. A. Aitken, J. Chem. Phys. **155**, 034308 (2021).
[7] M. H. Palmer, M. Coreno, M. de Simone, C. Grazioli, N. C. Jones, S. V. Hoffmann, and R. A. Aitken, J. Chem. Phys. **156**, 064305 (2022).
[8] C. A. Coulson and H. C. Longuet-Higgins, Proc. R. Soc. London, Ser. A **192**, 16–32 (1947).
[9] C. A. Coulson, Proc. Phys. Soc., London, Sect. A **65**, 933–945 (1952).
[10] H. H. Jaffe and M. Orchin, *Theory and Applications of Ultraviolet Spectroscopy* (Wiley, New York, NY, 1962), Chap. 13.9, pp. 337–344.
[11] R. G. Parr, *The Quantum Theory of Molecular Electronic Structure* (Benjamin, New York, NY, 1964), p. 58.
[12] G. M. Badger, "Aromatic character and aromaticity," in *Cambridge Texts in Chemistry and Biochemistry* (Cambridge University Press, 1969), ISBN: 9780521095433.
[13] L. Salem, *The Molecular Orbital Theory of Conjugated Systems* (W. A. Benjamin, New York, NY, 1966), Chaps. 1–5 and 1–6.
[14] R. Pariser, J. Chem. Phys. **25**, 1112–1116 (1956).
[15] H. J. Tobler, A. Bauder, and H. H. Günthard, J. Mol. Spectrosc. **18**, 239–246 (1965).
[16] S. Huber, G. Grassi, and A. Bauder, Mol. Phys. **103**, 1395–1409 (2005).
[17] M. B. Robin, *Higher Excited States of Polyatomic Molecules* (Academic Press, New York, NY, 1975), Vol. II, Chap. VI.B, p. 267.
[18] M. B. Robin, *Higher Excited States of Polyatomic Molecules* (Academic Press, New York, NY, 1975), Vol. III, Chap. XX, p. 379.
[19] G. R. Hunt and I. G. Ross, J. Mol. Spectrosc. **9**, 50–78 (1962).
[20] G. R. Hunt and I. G. Ross, Proc. Chem. Soc. 11–12 (1961).
[21] M. Orenstein, S. Kimel, and S. Speiser, Chem. Phys. Lett. **58**, 582–585 (1978).
[22] D. S. McClure, J. Chem. Phys. **22**, 1256–1257 (1954).
[23] J. W. Sidman and D. S. McClure, J. Chem. Phys. **24**, 757–763 (1956).
[24] T. Suzuki and M. Ito, J. Phys. Chem. **91**, 3537–3542 (1987).
[25] A. A. Ruth, E.-K. Kim, and A. Hese, Phys. Chem. Chem. Phys. **1**, 5121–5128 (1999).
[26] G. A. Kourouklis, K. Siomos, and L. G. Christophorou, J. Mol. Spectrosc. **92**, 127–140 (1982).
[27] P. Bałuk, A. Kawski, M. Kałas, and S. Jaśkiewicz, Z. Naturforsch., A **35**, 1421–1423 (1980).
[28] R. S. Chao and R. K. Khanna, Spectrochim. Acta, Part A **33**, 53 (1977).
[29] M. Beer and H. C. Longuet-Higgins, J. Chem. Phys. **23**, 1390–1391 (1955).
[30] A. J. Wurzer, T. Wilhelm, J. Piel, and E. Riedle, Chem. Phys. Lett. **299**, 296–302 (1999).
[31] J. C. del Valle and J. Catalán, Phys. Chem. Chem. Phys. **21**, 10061–10069 (2019).
[32] Y. Numata, S. Toyoshima, K. Okuyama, M. Yasunami, and I. Suzuka, J. Phys. Chem. A **113**, 9603–9611 (2009).
[33] G. D. Gillispie and E. C. Lim, J. Chem. Phys. **68**, 4578–4586 (1978).
[34] M. Fujii, T. Ebata, N. Mikami, and M. Ito, Chem. Phys. **77**, 191–200 (1983).
[35] M. J. Bearpark, F. Bernardi, S. Clifford, M. Olivucci, M. A. Robb, B. R. Smith, and T. Vreven, J. Am. Chem. Soc. **118**, 169–175 (1996).
[36] H.-P. Solowan, P. Malý, and T. Brixner, J. Chem. Phys. **157**, 044201 (2022).
[37] T. Kitagawa, Y. Harada, H. Inokuchi, and K. Kodera, J. Mol. Spectrosc. **19**, 1–3 (1966).
[38] L. B. Clark, J. Chem. Phys. **43**, 2566–2567 (1965).
[39] D. Bouler, W. S. Felps, J. Lewis, R. V. Nauman, and S. P. McGlynn, Chem. Phys. Lett. **67**, 420–423 (1979).
[40] J. W. Lewis, R. V. Nauman, D. B. Bouler, and S. P. McGlynn, J. Phys. Chem. **87**, 3611–3615 (1983).
[41] J. H. D. Eland and C. J. Danby, Z. Naturforsch., A **23**, 355–357 (1968).
[42] N. Kuthirummal and P. M. Weber, Chem. Phys. Lett. **378**, 647–653 (2003).
[43] N. Kuthirummal and P. M. Weber, J. Mol. Struct. **787**, 163–166 (2006).
[44] V. Blanchet, K. Raffael, G. Turri, B. Chatel, B. Girard, I. A. Garcia, I. Wilkinson, and B. J. Whitaker, J. Chem. Phys. **128**, 164318 (2008).
[45] H.-C. Hsu, J.-J. Lyu, C.-L. Liu, C.-L. Huang, and C.-K. Ni, J. Chem. Phys. **124**, 054301 (2006).
[46] D. E. Mann, J. R. Platt, and H. B. Klevens, J. Chem. Phys. **17**, 481–484 (1949).
[47] C.-L. Liu, H.-C. Hsu, J.-J. Lyu, and C.-K. Ni, J. Chem. Phys. **124**, 054302 (2006).
[48] A. Bergman and J. Jortner, Chem. Phys. Lett. **20**, 8–10 (1973).
[49] W. D. Lawrance and A. E. W. Knight, J. Phys. Chem. **94**, 1249–1267 (1990).
[50] P. M. Kozlowski, G. Rauhut, and P. Pulay, J. Chem. Phys. **103**, 5650–5661 (1995).
[51] J. M. L. Martin, J. El-Yazal, and J.-P. François, J. Phys. Chem. **100**, 15358–15367 (1996).
[52] B. N. Cyvin and S. J. Cyvin, Spectrosc. Lett. **15**, 549–555 (1982).
[53] M. A. Martin-Drumel, O. Pirali, Y. Loquais, C. Falvo, and Ph. Bréchignac, Chem. Phys. Lett. **557**, 53 (2013).
[54] J. R. Cable and A. C. Albrecht, J. Chem. Phys. **84**, 1969 (1986).
[55] M. Kalas, A. Kawski, and P. Baluk, Acta Phys. Pol., A **69**, 143–153 (1986).

[56]M. J. Frisch, G. W. Trucks, H. B. Schlegel, G. E. Scuseria, M. A. Robb, J. R. Cheeseman, G. Scalmani, V. Barone, G. A. Petersson, H. Nakatsuji, X. Li, M. Caricato, A. V. Marenich, J. Bloino, B. G. Janesko, R. Gomperts, B. Mennucci, H. P. Hratchian, J. V. Ortiz, A. F. Izmaylov, J. L. Sonnenberg, D. Williams-Young, F. Ding, F. Lipparini, F. Egidi, J. Goings, B. Peng, A. Petrone, T. Henderson, D. Ranasinghe, V. G. Zakrzewski, J. Gao, N. Rega, G. Zheng, W. Liang, M. Hada, M. Ehara, K. Toyota, R. Fukuda, J. Hasegawa, M. Ishida, T. Nakajim, Y. Honda, O. Kitao, H. Nakai, T. Vreven, K. Throssell, J. A. Montgomery, Jr, J. E. Peralta, F. Ogliaro, M. J. Bearpark, J. J. Heyd, E. N. Brothers, K. N. Kudin, V. N. Staroverov, T. A. Keith, R. Kobayashi, J. Normand, K. Raghavachari, A. P. Rendell, J. C. Burant, S. S. Iyenga, r J. Tomasi, M. Cossi, J. M. Millam, M. Klene, C. Adamo, R. Cammi, J. W. Ochterski, R. L. Martin, K. Morokuma, O. Farkas, J. B. Foresman, and D. J. Fox, GAUSSIAN 16, Revision A.03, Gaussian Inc., Wallingford CT, 2016.
[57]H. Nakatsuji and K. Hirao, Int. J. Quantum Chem. **20**, 1301–1313 (1981).
[58]H. Nakatsuji and T. Yonezawa, Chem. Phys. Lett. **87**, 426–431 (1982).
[59]H. Nakatsuji, Chem. Phys. **75**, 425–441 (1983).
[60]H. Nakatsuji, Int. J. Quantum Chem., Symp. **24**(S17), 241–255 (1983).
[61]H. Nakatsuji, K. Ohta, and T. Yonezawa, J. Phys. Chem. **87**, 3068–3074 (1983).
[62]V. Barone, J. Bloino, M. Biczysko, and F. Santoro, J. Chem. Theory Comput. **5**, 540–554 (2009).
[63]J. Bloino, M. Biczysko, F. Santoro, and V. Barone, J. Chem. Theory Comput. **6**, 1256–1274 (2010).
[64]A. Baiardi, J. Bloino, and V. Barone, J. Chem. Theory Comput. **9**, 4097–4115 (2013).
[65]R. G. Parr and W. Yang, *Density-functional Theory of Atoms and Molecules* (Oxford University Press, Oxford, 1989).
[66]A. D. Becke, J. Chem. Phys. **98**, 5648–5652 (1993).
[67]J. K. Labanowski and J. W. Andzelm, *Density Functional Methods in Chemistry* (Springer, Berlin, 1991).
[68]W. Kohn and L. J. Sham, Phys. Rev. **140**, A1133–A1138 (1965).
[69]T. Yanai, D. P. Tew, and N. C. Handy, Chem. Phys. Lett. **393**, 51–57 (2004).
[70]R. J. Buenker and S. Krebs, in *Recent Advances in Computational Chemistry 4*, Recent Advances in Multireference Methods, edited by K. Hirao (World Scientific Pub Co Inc, 1999), pp. 1–29.
[71]M. F. Guest, I. J. Bush, H. J. J. Van Dam, P. Sherwood, J. M. H. Thomas, J. H. Van Lenthe, R. W. A. Havenith, and J. Kendrick, Mol. Phys. **103**, 719–747 (2005).
[72]R. Krishnan, J. S. Binkley, R. Seeger, and J. A. Pople, J. Chem. Phys. **72**, 650–654 (1980).
[73]G. J. Small and S. Kusserow, J. Chem. Phys. **60**, 1558–1563 (1974).
[74]G. J. Small, J. Chem. Phys. **54**, 3300–3306 (1971).
[75]E. Heilbronner and K. Wieland, Helv. Chim. Acta **30**, 947–956 (1947).
[76]A. McHugh, D. Ramsay, and I. Ross, Aust. J. Chem. **21**, 2835–2845 (1968).
[77]R. Boschi, E. Clar, and W. Schmidt, J. Chem. Phys. **60**, 4406–4418 (1974).
[78]T. Kitagawa, J. Mol. Spectrosc. **26**, 1 (1966).
[79]See http://www.gnuplot.info for Gnuplot Release 5.0.7.
[80]Origin Version 2021b OriginLab Corporation, Northampton, MA, USA.
[81]GaussView Version 6.1, R. Dennington, T. A. Keith, and J. M. Millam, Semichem Inc. Shawnee Mission KS, 2016.